Chapter 4

APPLICATIONS

The aim of this chapter is to present some interesting applications of RTD Fluxgate magnetometers. The RTD Fluxgate can be considered as a suitable, low cost alternative to other technologies (in particular 2^{nd} harmonic Fluxgates and SQUID magnetometers) in situations where the resolution in the order of nT is required.

Moreover, the very good performances of the device together with its low cost and complexity, enable a set of new applications that would be otherwise impossible to implement.

4.1. Security

Magnetometers are an essential security tool and have been adopted by private and public business as a way to add a layer of protection to already existing security plans. By alerting security quickly, a magnetometer provides a crucial time element that allows for the best responses to contain any problems made by individuals carrying weapons attempting to enter a protected area.

The operating principle is straightforward: the presence of metallic objects in the environment alters the magnetic field in the nearby. The background magnetic field is usually produced by a controlled source (an array of electromagnets, for example). However, the geomagnetic field, always present in an unshielded environment, can be exploited for the purpose, as a simpler and more convenient alternative.

In order to quantitatively evaluate the performances of the RTD Fluxgate these kind of situations, the theory of binary prediction has been used.
In the following section, ROC curves are introduced and discussed as a convenient and common-accepted way to quantify the performance of binary classifiers.

4.1.1. ROC Curves

In a simple two-class prediction problem (positives and negatives classes) the classifier is demanded to map each instance (i.e. samples to be classified) to one of the two classes. Given an instance set and a classifier, there are four possible outcomes:

- True positive, if the instance is positive and it is classified as positive
- False negative, if the instance is positive and it is classified as negative
- True negative, if the instance is negative and it is classified as negative
- False Positive, if the instance is negative and it is classified as positive

In particular, we can define the True Positive Rate (TPR) as the ratio between the number of true positives and the total positives and the False Positive Rate (FPR) as the ratio between the number of false positives and the total negatives.

In signal detection theory a Receiver Operating Characteristic (ROC) Curve is a 2D graphical plot of the TPR (sensitivity) vs. FPR (1-specificity) for a binary classifier system, as its discrimination threshold is varied. ROC graphs are used to depict the trade-off between hit rates (benefits) and false alarm rates (costs) of classifiers [4.1.1-4.1.3].

In our case, the binary classifier is the RTD Fluxgate magnetometer and the instances are the samples of its output signal (the Resi-

dence Times Difference, as stated above). The procedure that has been followed to draw ROC curves can be summarized in these simple steps:

- Fixing the operating conditions (the target and the sensor's excitation waveform parameters) and recording the RTD evolution
- Plotting the RTD samples distribution in the presence and in the absence of the target
- For different values of the discrimination threshold estimating the True Positive Rate and the False Positive Rate

Often, to easily compare classifiers, ROC curves are reduced to a single scalar value representing expected performance: the Area Under Curve (*AUC*). Since the *AUC* is a portion of the area of the unit square, its value will always be between 0 and 1.0.

However, because random guessing produces the diagonal line between (0; 0) and (1;1), which has an area of 0.5, no realistic classifier should have an *AUC* less than 0.5. An example of a typical ROC curve is given in Fig. 4.1.1 and Fig. 4.1.2.

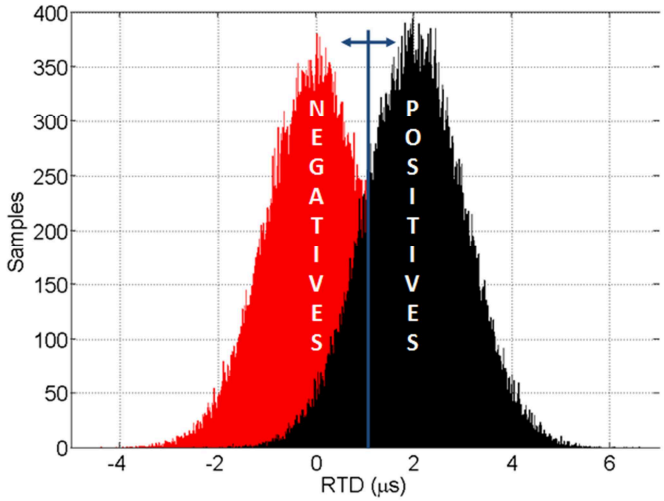

Figure 4.1.1 - Qualitative example of *RTD* samples distribution in ROC analysis. The red and the black curves represent, respectively, the sensor output in absence and in presence of the target.

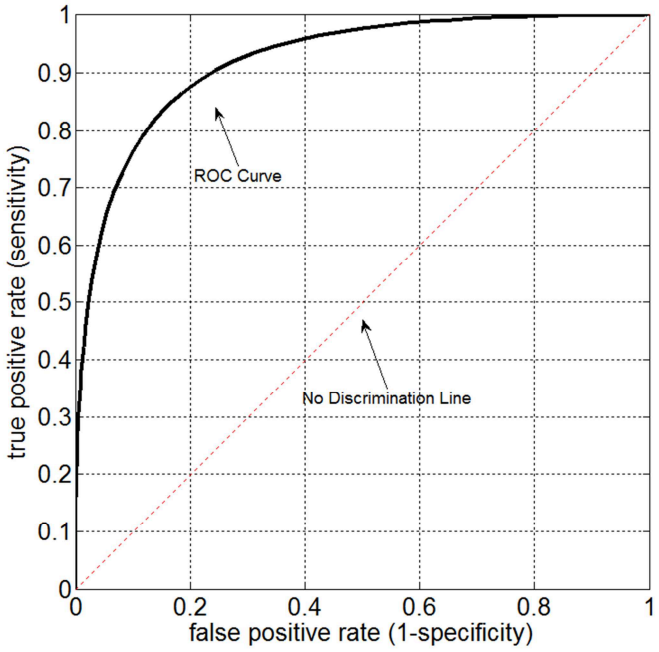

Figure 4.1.2 - Example of a typical ROC curve starting from data represented in Figure 1. The *No Discrimination Line* represents the strategy of randomly guessing a class

4.1.2. Experimental Results

The experimental setup is schematically shown in Fig. 4.1.3. Because of the high spatial resolution of the μWire Fluxgate prototype the target has been finely aligned with the sensor axis by the use of a laser pointer (Fig. 4.1.4)

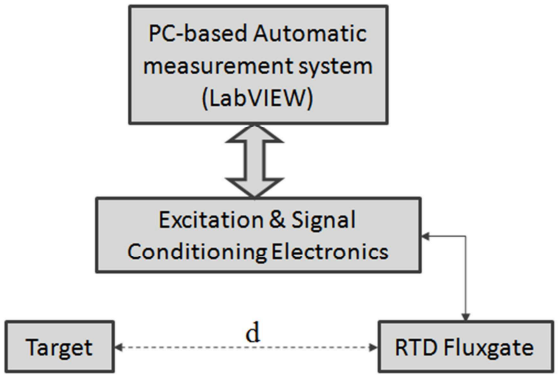

Figure 4.1.3 - Experimental setup overview.

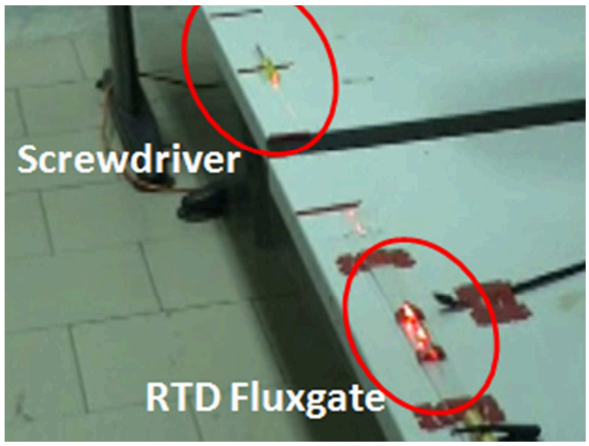

Figure 4.1.4 - The target has been finely aligned with the sensor axis by the use of a laser pointer.

Tests have been performed with different common-use metallic objects placed at different distances from the magnetometer. Results on the detection of a screwdriver are reported in Fig. 4.1.6.
The ROC curve for a distance of 75cm give us $AUC = 1$; this means that exists at least one value for the discrimination threshold that give us $TPR = 1$ and $FPR = 0$ (top-left corner).
In this first case the two *RTD* distribution (see Fig. 4.1.1) does not overlap. As the distance increases the performance of the classifier begin to get closer to the no discrimination line and the *AUC* decreases accordingly. For distances greater than 2 meters the analysis of the *RTD* distribution can't give us any information about the presence of the metallic target.

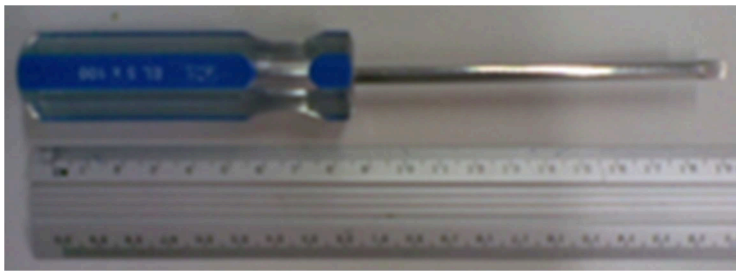

Figure 4.1.5 - The screwdriver used for the experimental tests. Results are reported in Fig. 4.1.6.

The results reported in Fig. 4.1.6 demonstrate the feasibility of using RTD- fluxgate for B-field measurement in security applications.
Further investigations about optimal operating conditions and sensor structure could improve the device performance in terms of resolution thus leading to an effective, low cost system to detect metallic targets in unshielded environment at room temperature.

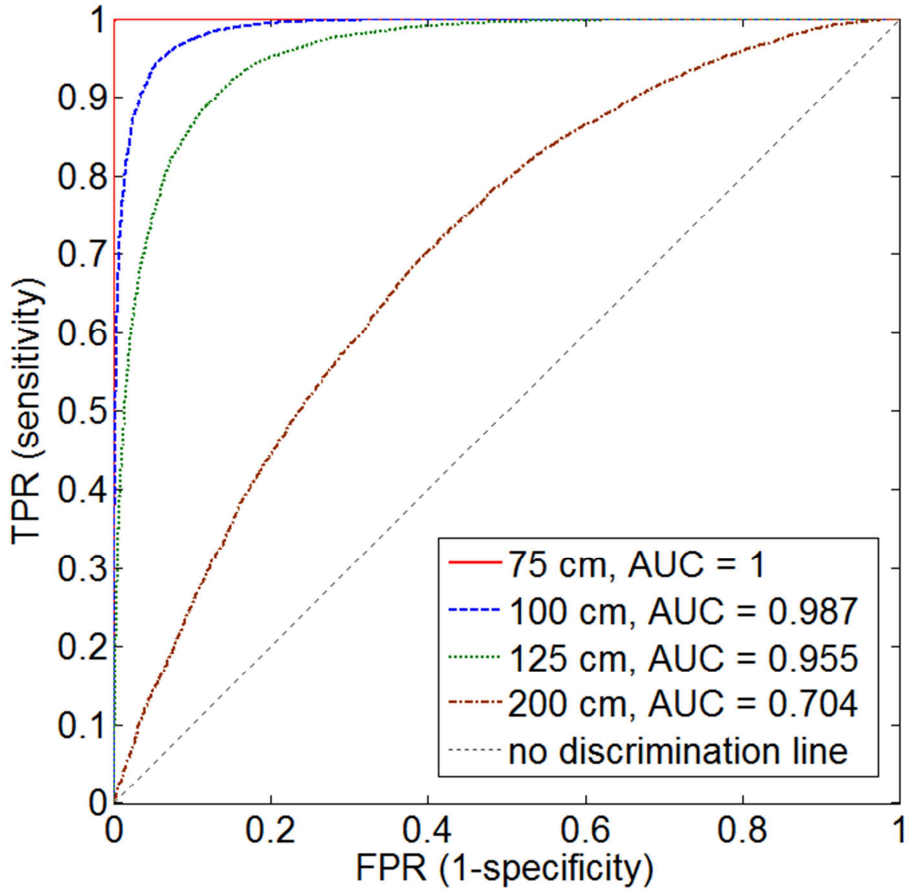

Figure 4.1.6 - ROC Curves for different distance values of the target.

4.2. Magnetic Immunoassay

Magnetic bioassay is becoming of great interest due to advances in magnetic materials and in high sensitive detection techniques [4.2.1]. The main idea behind these techniques is the possibility of labeling target bio-entities with magnetic particles performing direct or indirect tasks. A large ensemble of magnetic particles is available which differs in magnetic properties, sizes and biocompatibility properties.

Particles with sizes ranging from a few nanometers up to tens of nanometers are available, which make them comparable to the biological entity of interest like a cell (10–100 μm), a virus (20–450 nm), a protein (5–50 nm) or a gene (2 nm wide and 10–100 nm long). For larger size target cells both magnetic nanoparticles and larger particles can be used. To this end microspheres (agglomerations of sub-micron sized magnetic particles) represents a convenient solution [4.2.2].

Labeling is made possible usually through coating the magnetic particles surface with biocompatible molecules providing a link between the particle and the target site on a cell or molecule. A large number of coatings are commercially available.

Target cells are usually targeted by antibodies or other biological macromolecules binding to their matching antigen. For example, magnetic particles coated with immune-specific agents have been successfully bound to red blood cells [4.2.3, 4.2.4], lung cancer cells [4.2.5], bacteria [4.2.6] and other target entities [4.2.7-4.2.8].

Actually, several applications in the field of magnetic bioassay have been identified of which magnetic separation, drug delivery, hyperthermia treatments, magnetic resonance imaging (MRI) and magnetic labeling are a limited number of examples.

In separation task the magnetically labeled material is separated from its native solution by applying a magnetic force conveying the target entities into the inspection site. Aims of drug delivery are the reduction of side effects caused by the systemic distribution of traditional pharmacological therapy and dosage reduction by a specific drug localization. As an example, in cancer therapy, usually

a cytotoxic drug is conveyed to the target site by a biocompatible ferrofluid carrier.
Concerning hyperthermia treatments the use of magnetic labeling allows to fix the unsustainable heating of healthy tissue of traditional techniques. Magnetic particles as contrast agent in MRI are used for the localization of brain and cardiac infarcts, liver lesions or cancers. There are several commercially available magnetic contrast agents such as dextran coated super-magnetic iron oxide which are biocompatible and are excreted via the liver after the treatment. The particles used are magnetically saturated in the normal range of magnetic field strengths used in MRI scanners, thereby establishing a substantial locally perturbing dipolar field.
Magnetic biosensing techniques can be used to localize target entities. In this case, after labeling the target entities a remote sensing approach must be adopted. The most common techniques are AC susceptometry or SQUID magnetometry [4.2.9-4.2.10]. Although these schemes allow high sensitive, main drawbacks are related to expensive cryogenics and instrumentation.
Alternative solutions use giant magneto resistance sensor (GMR) which presents a resistance varying with the applied magnetic field [4.2.11]. Although these device are nominally less sensitive than SQUID magnetometers, the extreme proximity of the sensor to the inspected entities tagged by magnetic beads could dramatically boost its performance.
In this section, preliminary results concerning the use of RTD-Fluxgate as candidate for magnetic beads detection in bioassay application are given.

4.2.1. The Experimental Setup

4.2.1..1 Hardware

For the experimental tests the following hardware has been used:

- μWire RTD Fluxgate magnetometer
- μController-based electronic circuit for the driving and the conditioning of the sensor

- A suitable, magnetic-transparent mechanical structure
- A set of magnets
- Various commercially available samples of ferrofluid, used as magnetic markers.

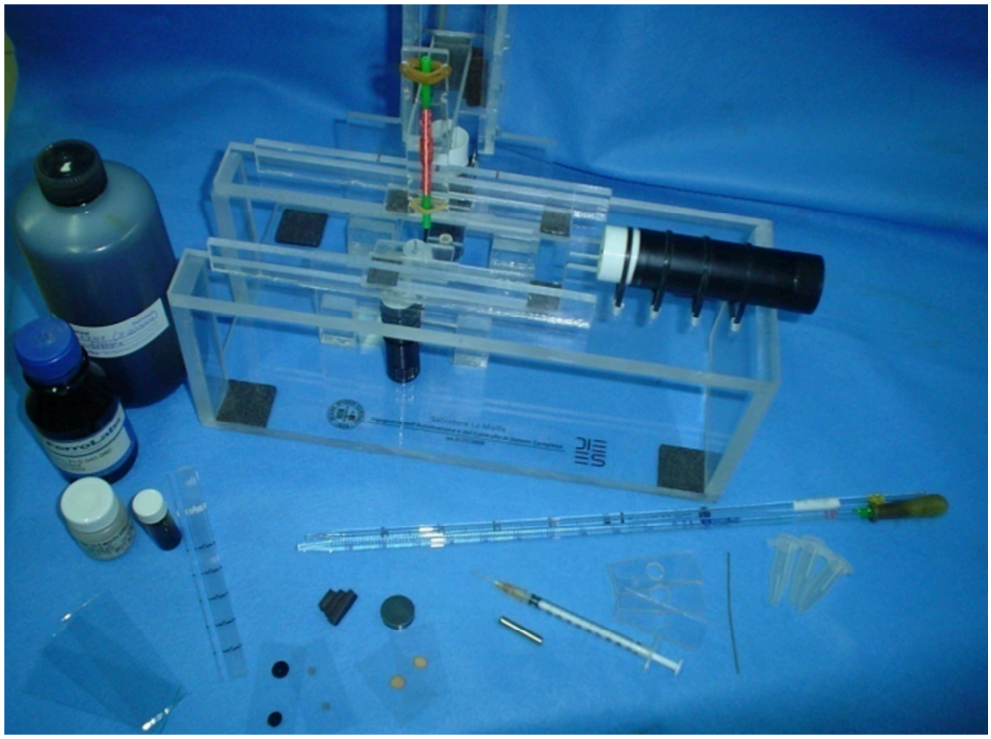

Figure 4.2.1 - Overview of the hardware setup used for the experimental tests

The measurement procedure can be briefly described as follows: a series of targets, consisting of known amount of volume of magnetic tracers suspension, are deposited on common laboratory glass slides by means of calibrated capillary.
The fluxgate magnetometer is maintained in an upright position, aligned with a suitable magnet that is needed for the magnetization of the paramagnetic sample. During each measure step, the slide is forced to move perpendicular to the axis of the fluxgate; when the volume of the magnetic tracer passes at the sensor, an output signal proportional to volume of tracer deposited on the slide can be observed.

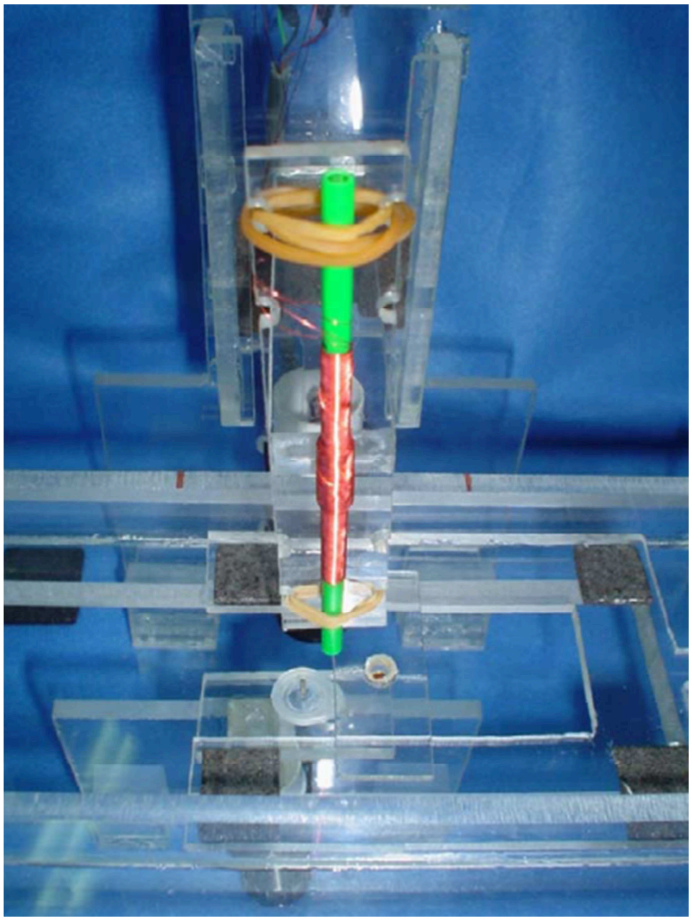

Figure 4.2.2 - Arrangement of the RTD fluxgate compared to the slide and the permanent magnet.

In order to ensure repeatability of the procedure just described, it's crucial to have a support structure with the following features:

- It must provide a stable support for the sensor, the slides and the permanent magnet
- It must allow the relative motion of the three parts
- It must be magnetically transparent (no metal parts)

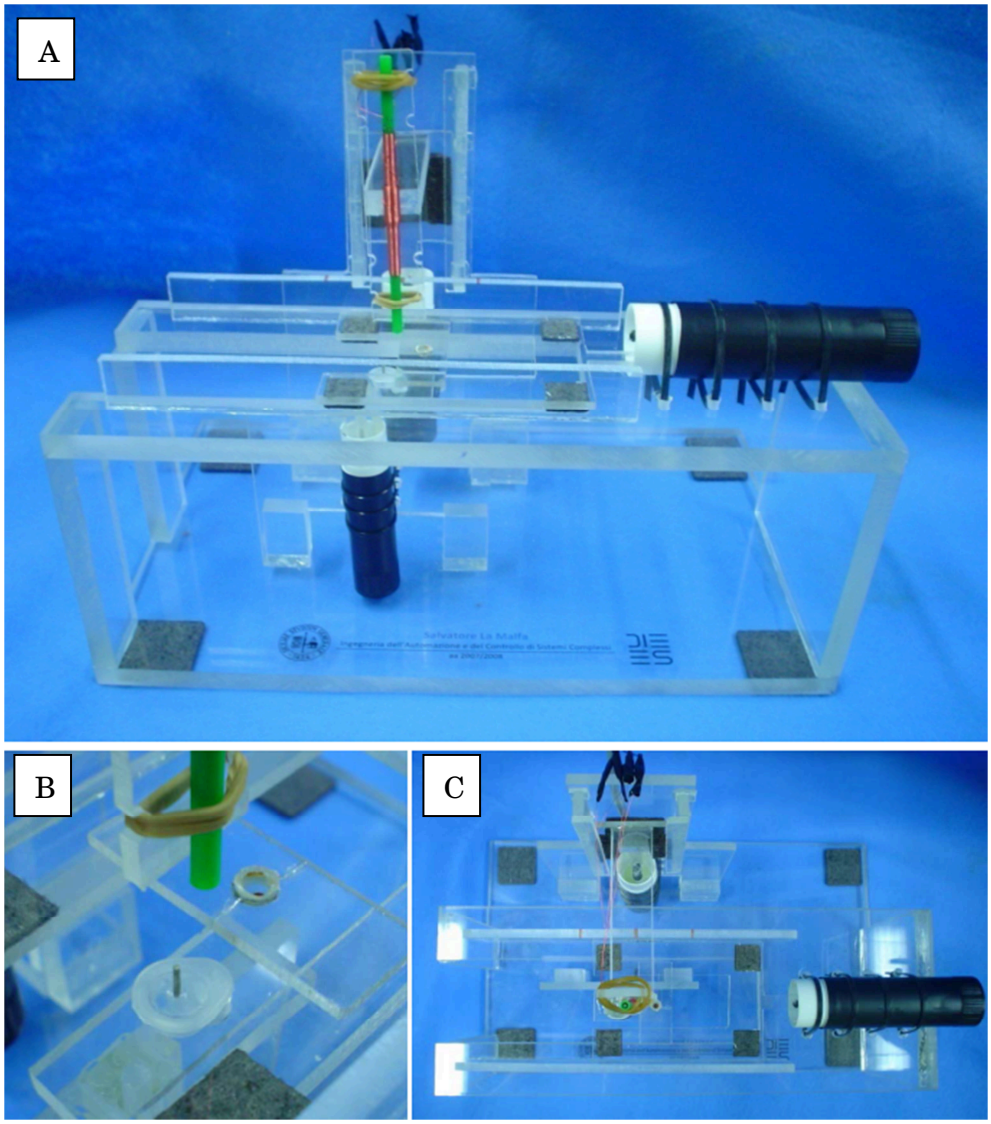

Figure 4.2.3 - (A) Overview of the support structure made of Plexiglas. (B) Details of the sensing area. (C) top view

For what concerns the magnetic tracers used in experimental tests, several different samples of commercially available products have been evaluated (Table 4.2.1):

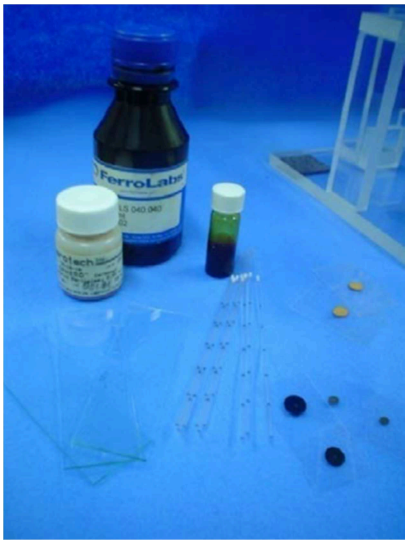

Figure 4.2.4 - Overview of some of the magnetic tracers used in the experimental tests.

The features of interest in the case of magnetic markers for immunoassay applications are primarily the size and sometimes the percentage of magnetite when dealing with heterogeneous particles (e.g. Spherotech). By following these quality parameters, ferrofluids appears to be the ideal material for this purpose.
In fact, they feature the smaller particles among all commercial products (about 10 nm in diameter) and consist of magnetite to 100%.
Ferrofluids provide a valuable signal even for small volumes and allow the identification and / or separation or biological components of comparable size to those of the particles.

Vendor	Product code	Description
Ferrotec	EFH1	Ferrofluid, suspension of magnetite particles (diameter ≈ 10 nm) stabilized by oleic acid in synthetic oil. Saturation magnetization = 40mT, viscosity = 6 mPa.s, density = 1.21 g/cm3

Ferrotec	APGE26	Ferrofluid, suspension of magnetite particles (diameter ≈ 10 nm) stabilized by oleic acid in synthetic oil. Saturation magnetization = 2.75±10% mT, viscosity = 300 ± 10% mPa.s, density = 1.11 g/cm3
Ferrolabs	FLS-040-040	Ferrofluid, suspension of magnetite particles (diameter ≈ 10 nm) stabilized by oleic acid in silicon fluid. Saturation magnetization = 50k A/m, viscosity = 800 mPa.s,
Spherotech	CM-10-10	Magnetic particles consisting of magnetite distributed in a core of polystyrene (magnetite up to 15%), diameter = 1÷1.4 μm. Concentration of particles = 29.47 e6 / μl
Spherotech	SVM-10-10	Magnetic particles consisting of magnetite distributed in a core of polystyrene (magnetite up to 15%), diameter = 1÷1.4 μm. Coated with a Streptavidin layer. Concentration of particles = 5.895 e6 / μl

Table 4.2.1 - Key features of the tracers used in the tests.

The Ferrotec EFH1 contains spherical magnetite particles (Fe2O3) with a diameter of 10 nm. Therefore, each particle occupies a volume equal to:
The manufacturer declares a magnetite content from 3% to 15% of the total volume.
Considering that 1mm = 1ul we have the following concentrations, assuming a volume fraction equal to 3, 9, 15% (Table 4.2.2).

% in volume of Fe2O3	**Particles concentration in 1 μl**
3%	3.820e5
9%	1.146e6
15%	1.910e6

Table 4.2.2 - Estimated concentration of particles per microliter for the Ferrotec EFH1 ferrofluid

Now we compare these results with data reported by Spherotech about two of their products:

Spherotech	Particles concentration in 1µl	Equivalent conenctration
CM-10-10	29.47e6	3.536e6
SVM-10-10	5.895e6	7.074e5

Table 4.2.3 - Concentrations indicated by the manufacturer (Spherotech)

It 'was shown an “equivalent” concentration of particles, whereas in this type of particles, only 10 to 15% of the volume consists of magnetite, the rest is polystyrene.
Assuming an average distribution of magnetite of 12% we can derive an equivalent concentration, a more directly comparable parameter with EFH1.
As can be seen in any case, the concentrations are comparable, and this therefore justifies the interest in the use of ferrofluids in biomedical applications.

Following the considerations just made, we can estimate the number of particles that actual contribute to the magnetic signal.

The spatial resolution of a fluxgate is closely related to the geometry of the ferromagnetic core. Using a µWire RTD fluxgate, with a FeSiB core with a diameter of 100 microns, we therefore expect a spatial resolution rather close to 100 microns. This is obviously due to the high permeability of the FeSiB that the surrounding medium (Air and plastic) which is the preferred path for the flux lines.
From a practical standpoint, the ferrofluid used for measurements is placed inside a plastic container with size and shape approximating a hemisphere with a radius of 2.5 mm (Fig. 4.2.5)

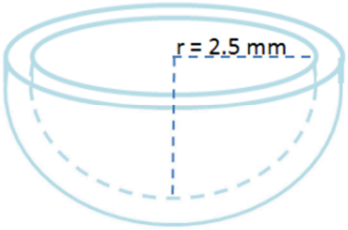

Figure 4.2.5 - schematization of the plastic container used for experimental measurements

So considering a concentration of magnetic particles equal to 9% of volume (1.146 e6/µl), taking into account the nominal spatial resolution of 100 µm of our device, we can calculate the number of particles actually involved in the useful signal:

The height reached by the ferrofluid as a function of its volume is calculated by solving the equation:

$$h^3 - 3rh^2 + \frac{3V_{ff}}{\pi} = 0$$

Obtained from the well-known formula for calculating the volume of a spherical cap:

$$V_{KS} = \frac{h^2\pi}{3}(3r - h)$$

Where h is our unknown, r is the radius of the hemisphere and V_{ff} the considered volume of ferrofluid.

Solving the equation for the volumes [0.5, 1, 2, 3, 4, 5] µl and considering only the particles contained in the cylinder with a diameter of 100 microns and height calculated according to the above equation, we obtain: (Table 4.2.4)

Ferrofluid volume (μl)	Height (mm)	Equivalent cylindrical volume (nl)	Actual number of particles (x1000)
0.5	0.257	8.07	4.63
1	0.366	11.5	6.6
2	0.523	16.4	9.4
3	0.646	20.3	11.6
4	0.752	23.6	13.6
5	0.847	26.6	15.2

Table 4.2.4 – Actual number of particles for a given EFH1 ferrofluid target volume

Then we observe that the number of particles detected by the sensor is sufficiently small.

The calculation just outlined, although approximate, has allowed us to evaluate the order size of the particles actually involved in the process of sensing starting from the considered volume of ferrofluid.

4.2.1..2 Software setup

The previously discussed μController excitation and conditioning circuit greatly simplifies the software for the monitoring and archiving of experimental measurements.
A LabVIEW virtual instrument with the following features has been realized:

- Manages the bidirectional serial communication with the board
- Allows real time monitoring of the signal from the sensor with settable time window
- Manages the datalog on ASCII files.

Below is a brief description of the LabVIEW GUI, with reference to Fig. 4.2.6:

A. RS-232 communication parameters
B. List of commands provided for setting the parameters of the signal
   excitation (serial 1) and those related to digital elaboration of the RTD performed by the μController (serial 2)
C. Input command panel and board status monitor
D. Calculation of the parameters serial1 as a function of the desired frequency and amplitude for the driving signal.
E. Path to log files
F. Parameters related to the observation time and the time window for
   the moving average
G. Graphic monitoring of raw and averaged RTD signals over the considered time-window

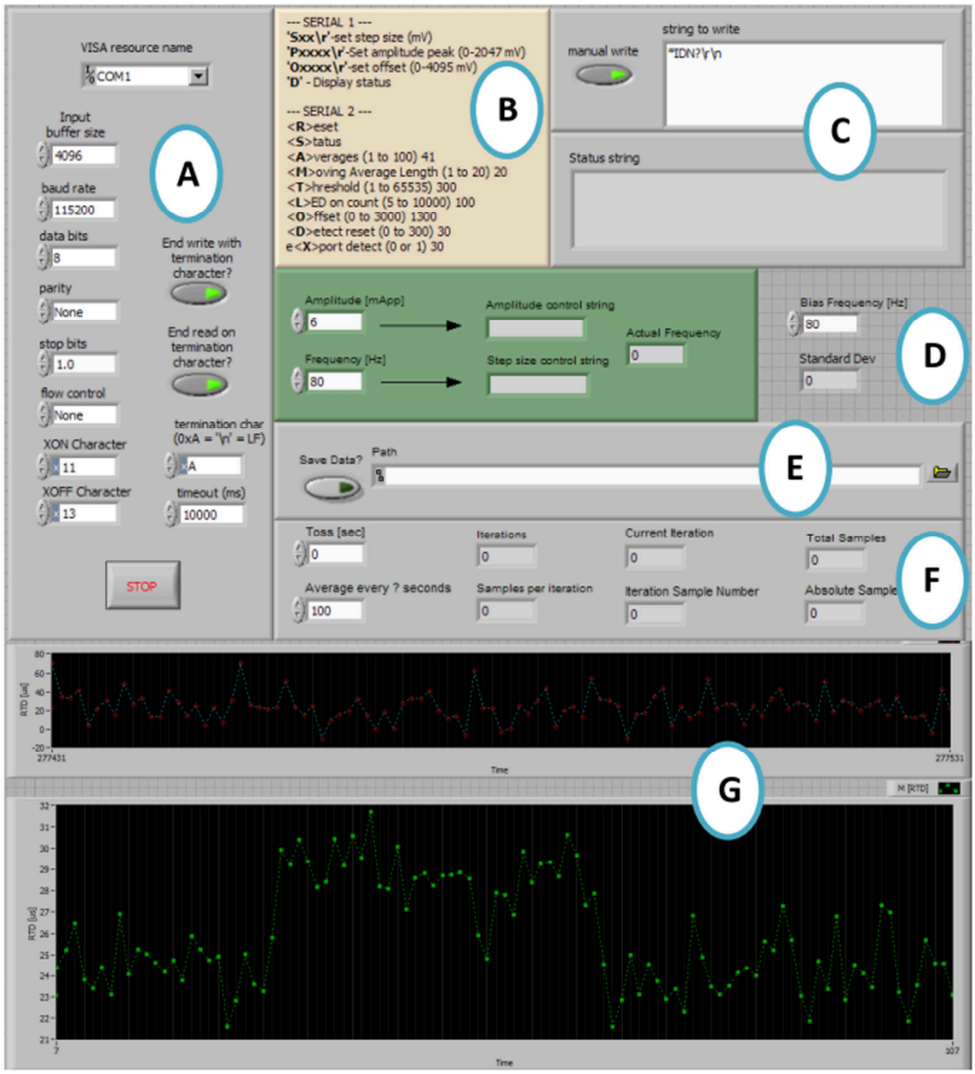

Figure 4.2.6 - Overview of the software developed for the data acquisition.

4.2.2. Experimental Results

In this chapter the experimental results will be reported and discussed.
In order to obtain a good resolution also for short observation times, a specific operating condition of the μWire RTD fluxgate has been chosen: 16.8mApp @ 80 Hz.
A preliminary characterization of sensor has been performed in order to estimate the resolution of the magnetometer in the working (unshielded) environment.
A resolution of 0.5nT @ 15s and less than 0.1nT @ t = 30 s has been observed. We have very good performance even for short time observation (<5s) which allows the sensor to use in dynamic applications, as in the case of slowly varying target.
These values are quite different with respect to those discussed in chapter 2 because in this case, the out-of-the-shield resolution has been evaluated.
After the characterization phase were carried out a number of tests various concentrations of magnetic tracers (see 4.2.1).
The measures are presented below are related to the use of ferrofluid EFH1 produced by Ferrotec, the results can be classified as follows:

- Static measurements (Tobsv = 30s)
- Repeatability tests
- Dynamic measurements (Tobsv = 0.5 s)

4.2.2..1 Static measurements

The static measurements were performed to characterize statically the sensor response to various amounts of ferrofluid (5, 4, 3, 2, 1, 0.5) μl
Each measure has a duration of 110s, divided as follows:

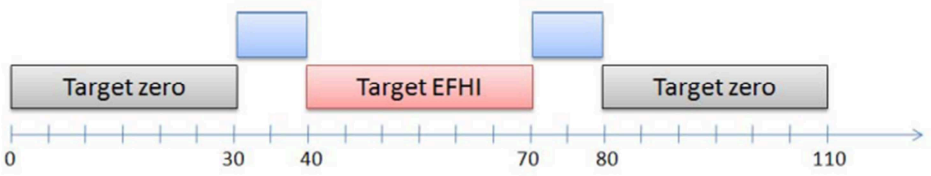

Figure 4.2.7 – Static measurements timeline schematization.

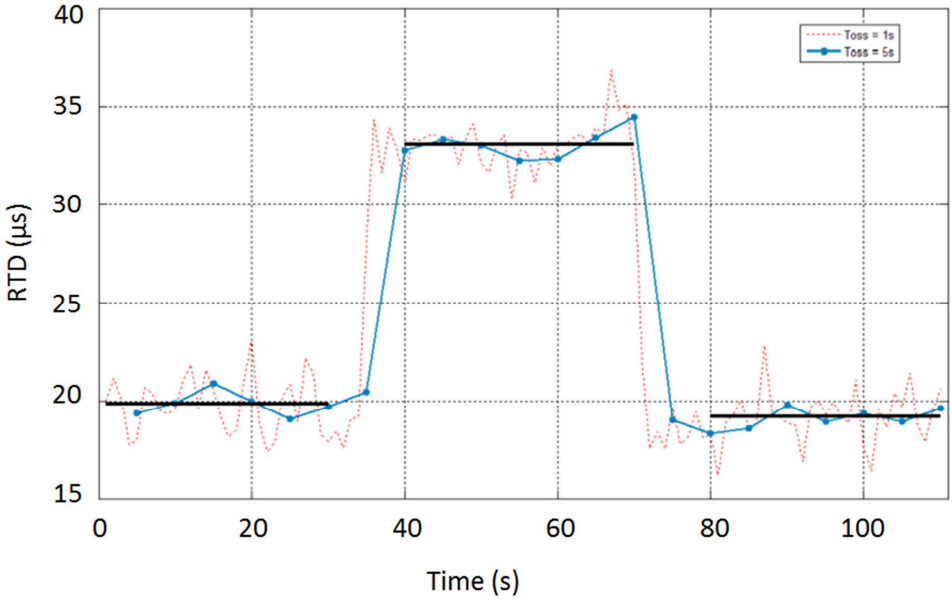

Figure 4.2.8 – Static measure for 5•l

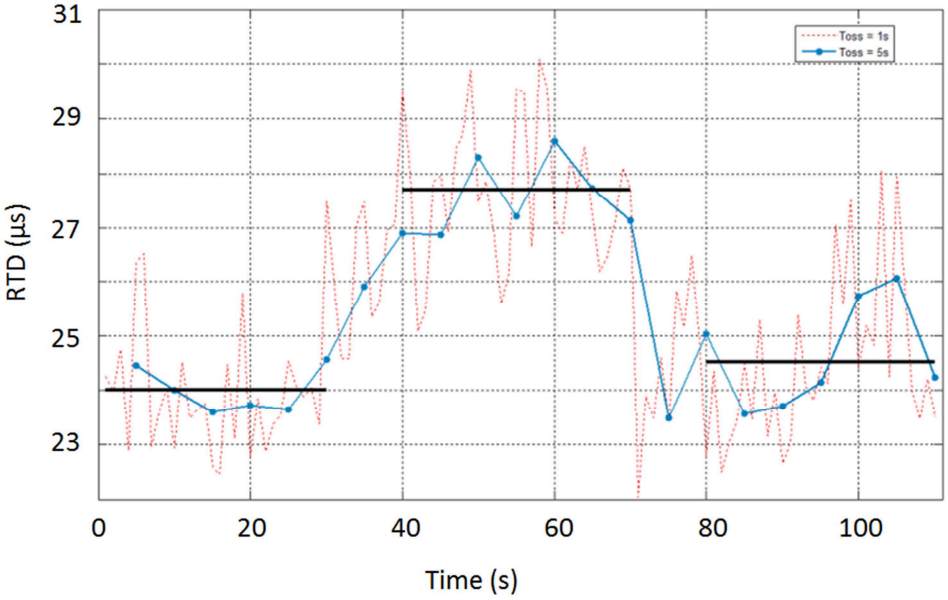

Figure 4.2.9 – Static measure for 0.5•l

The end of the fluxgate facing the target is 4 mm from the spot. the magnet used to polarize the magnetic particles is placed at a distance of about 1mm from the ferrofluid drop.
The figure 4.2.9 shows a well-defined signal even for a volume of 0.5µl. With reference to figures 4.2.8 and 4.2.9, the dashed curve in red represents the trend of the RTD at every 1s, the one in blue every 5s while the black segments represent the average RTD within 30s-regions.

4.2.2..2 Repeatability tests

In order to test the short-term repeatability of static measurements 3 consecutive tests have been performed for each volume of ferrofluid in the same operating conditions.

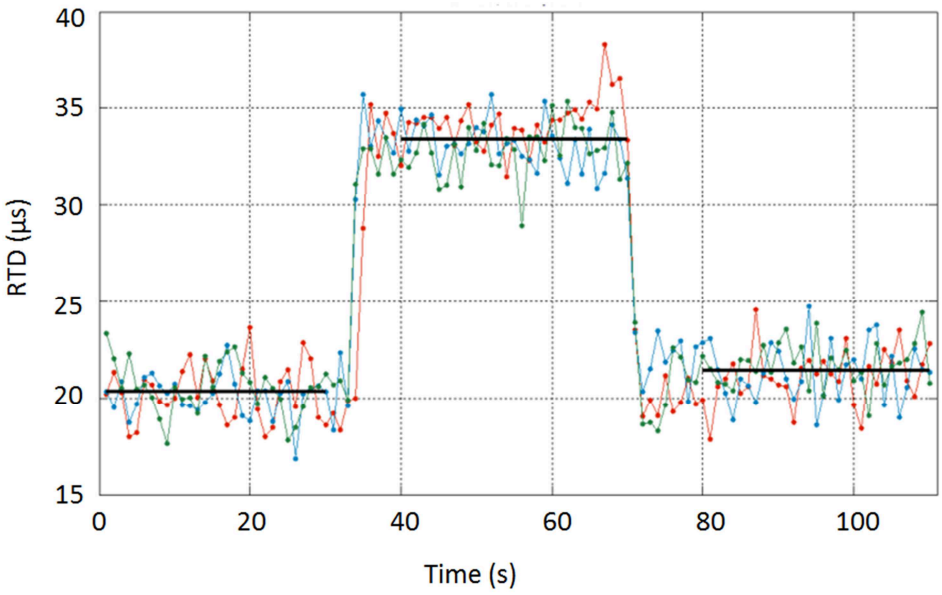

Figure 4.2.10 – Repeatability test for 5•l

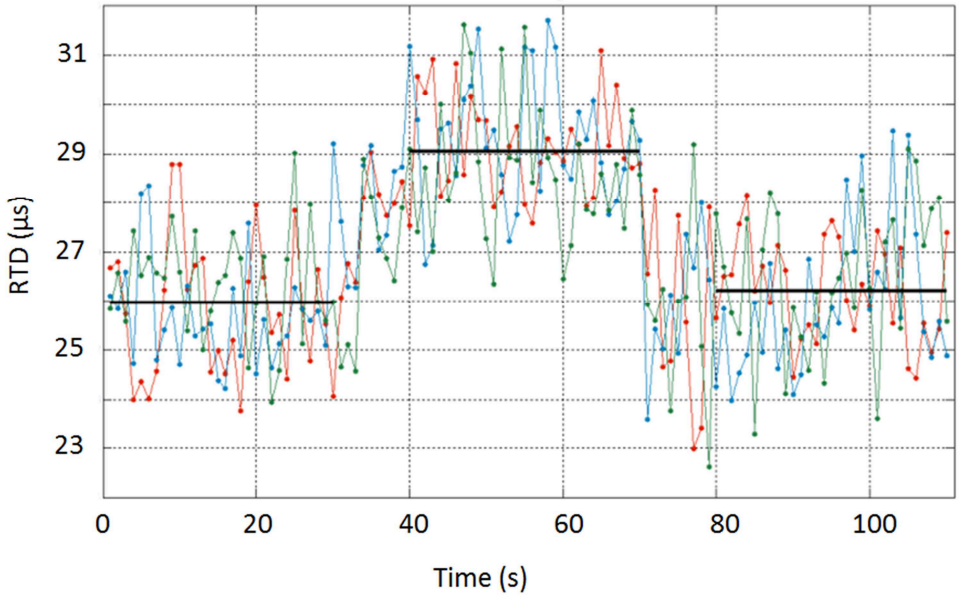

Figure 4.2.11 – Repeatability test for 0.5•l

What is easily observed that, even in the worst case considered (0.5 l), the output signal is definitely repeatable, and this is in line with the margin of resolution to present an observation time of 30 seconds.

4.2.2..3 Dynamical measurements

The preliminary study on the use of a fluxgate magnetometer in immunoassay applications cannot disregard a rough description of a possible setup for the measurement of the signal coming from various spots distributed on the substrate.
Let us suppose a structure similar to that shown in Fig. 4.2.12:

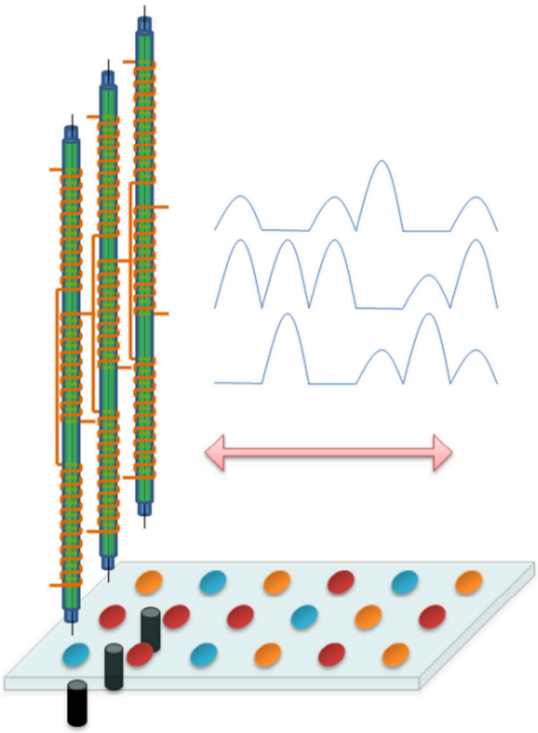

Figure 4.2.12 - Outline of a possible setup for the parallel spots readout. The spots shown in red are those with a large concentration of analyte, those indicated in orange have an average concentration, those in blue are analyte-free.

We have a number of spots distributed on the surface of a substrate, each site of an immunoassay process. At the steady state, we will have a number of magnetic markers anchored to the substrate, which will produce, if properly magnetized, a signal whose intensity is proportional to the concentration of the analyte in the relative spot.

With reference to Fig. 4.2.12, let's suppose to have a number of fluxgate in a comb-like configuration, in line with an equal number of magnets for the magnetization of the markers. By imposing a constant speed to the structure (or similarly, by keeping the structure fixed and moving the substrate) we will have a total signal that provides information on the field distribution between various spots, and finally on the concentration of the analyte.

We can imagine to apply this procedure in transient measurements, providing valuable information on the nature of the chemical links to the biologist as well as on their number; this perspective is what most distinguishes a readout strategy based on magnetic markers compared to traditional methods (e.g. fluorescence).

To test the feasibility of this system, some dynamic measurements have been performed, that is, subjecting the slide containing the target to a triangular velocity profile with an amplitude of about 0.5 cm/s, with respect to the fluxgate magnetometer, fixed in perpendicular position. The results are shown in Fig. 4.2.13 and 4.2.14.

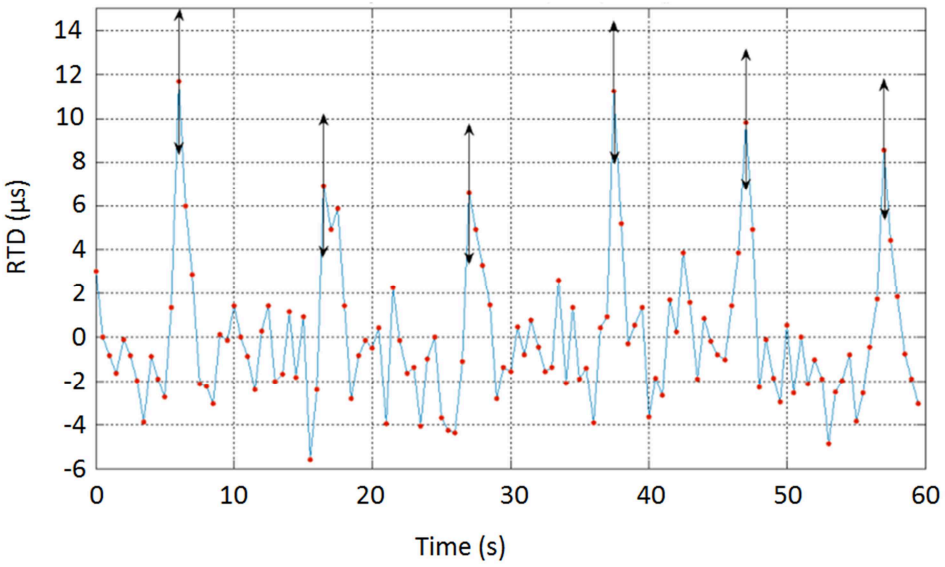

Figure 4.2.13 – Dynamic measurement for 4•l

The signals are filtered by considering a time window of 0.5 s. In correspondence to the passage of the spot along the axis of the fluxgate, a peak in the output signal is obtained whose intensity is proportional to the number of particles present in the target solution.

For each peak, the uncertainty ranges at 95.0% has been indicated in the graphs.

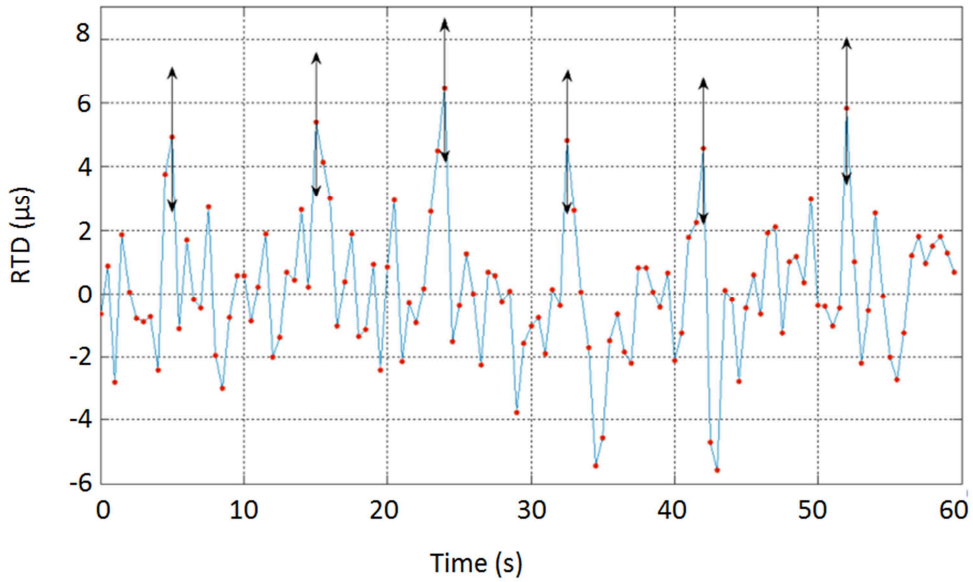

Figure 4.2.14 – Dynamic measurement for 0.5•l

We observe that only in the worst case considered (V = 0.5 µl) peaks are at limits of resolution. This behavior could be improved by decreasing then target-fluxgate relative velocity (which corresponds exactly to increase the observation time and then taking advantage of a better resolution).

Describing the substrate as an array of spots, if the chemical phenomenon in each spot has a dynamic that evolves with a speed less than or equal to the scanning speed of the fluxgate divided by the number of columns of the matrix, then we are able to measure the transient of the entire process.

Otherwise one will need to act on the scanning speed that is limited by the resolution of the sensor. A device capable of good resolution even for very short times of observations is obviously crucial in this kind of application.

4.2.3. Conclusions

The aim of this work has been to evaluate the behavior of RTD Fluxgates in biomedical applications.
The focus has been on the possible use of fluxgates in conjunction with magnetic particles (ferrofluids, in particular), with an average diameter of 10nm, functionalized with appropriate biomolecules depending on the particular chemical target.
This represents an alternative strategy to classical fluorescence for DNA microarray sequencing, as magnetic particles are used rather than the classic fluorescent markers.
One of the main reasons for this last point is the opportunity given by the evaluation of the transient magnetic reading the phenomenon of hybridization of DNA. This is extremely important for researchers in the field of DNA sequencing, and this problem has not yet been fully resolved in the scientific community.
In this sense, the proposed setup together with the dynamic measurements confirm the validity of the proposed approach.

References

[4.1.1] T. Fawcett, “ROC graphs: notes and practical considerations for data mining researchers”, HP Technical Report HPL-2003-4, HP Laboratories, 2003.
[4.1.2] D. Hand and R. J. Till, “A simple generalization of the area under the ROC curve for multiple class classification problems”, Machine Learning, Vol. 45, 171-186, 2001.
[4.1.3] Zeng-Chang Qin, ROC analysis for predictions made by probabilistic classifiers, Proceedings of the Fourth International Conference on Machine Learning and Cybernetics, Guangzhou, 18-21 August 2005
[4.2.1] Q A Pankhurst1, J Connolly2, S K Jones3 and J Dobson, Applications
of magnetic nanoparticles in biomedicine, J. Phys. D: Appl. Phys. 36 (2003) R167–R181, IOP Journ. Phys. D: Appl. Physics.
[4.2.2] Ugelstad J, Prestvik W S, Stenstad P, Kilaas L and Kvalheim G 1998
Selective cell separation with monosized magnetizable polymer beads Magnetism in Medicine ed H Nowak (Berlin: Wiley-VCH) pp 471–88
[4.2.3] Molday R S and MacKenzie D 1982 Immunospecific ferromagnetic
iron–dextran reagents for the labeling and magnetic separation of cells J. Immunol. Methods 52 353–67
[4.2.4] Tibbe A, de Grooth B, Greve J, Liberti P, Dolan G and Terstappen L
1999 Optical tracking and detection of immunomagnetically selected and aligned cells Nature Biotechnol. 17 1210–13
[4.2.5] Kularatne B Y, Lorigan P, Browne S, Suvarna S K, Smith M O and
Lawry J 2002 Monitoring tumour cells in the peripheral blood of small cell lung cancer patients Cytometry 50 160–7
[4.2.6] Morisada S, Miyata N and Iwahori K 2002 Immunomagnetic
separation of scum-forming bacteria using polyclonal antibody that recognizes mycolic acids J. Microbiol. Methods 51 141–8

[4.2.7] Zigeuner R E, Riesenberg R, Pohla H, Hofstetter A and Oberneder R
2003 Isolation of circulating cancer cells from whole blood by immunomagnetic cell enrichment and unenriched immunocytochemistry in vitro J. Urol. 169 701–5
[4.2.8] Mura C V, Becker M I, Orellana A and Wolff D 2002
Immunopuri.cation of Golgi vesicles by magnetic sorting J. Immunol. Methods 260 263–71
[4.2.9] C.B. Kriz, K. Radevik, D. Kriz, Anal. Chem. 68, 1996
[4.2.10] R. Kotiz, H. Matz, L. Trahms et al., IEEE Trans. Appl. Supercond., 7,
3678, 1997
[4.2.11] M.M. Miller, P.E. Sheehan, R.L. Edelstein, C.R. Tamanaha, L.
Zhong, S. Bounnak, L.J. Whitman, R.J. Colton, A DNA array sensor utilizing magnetic microbeads and magnetoelectronic detection, Journ. of Magnetism and Magnetic Materials, 225, 138-144, 2001